TA 8.

FORSCHUNG - AUSBILDUNG - WEITERBILDUNG

Bericht Nr. 92

AN ADAPTIVE WAVELET GALERKIN ALGORITHM FOR ONE AND TWO DIMENSIONAL FLAME COMPUTATIONS

J. Fröhlich, K. Schneider

UNIVERSITÄT KAISERSLAUTERN
Fachbereich Mathematik
Postfach 3049

D-67653 Kaiserslautern

An adaptive Wavelet Galerkin Algorithm for one and two dimensional flame computations

J. Fröhlich, K. Schneider

July 19, 1993

Abstract

This paper is concerned with the development of a self-adaptive spatial discretization for PDEs using a wavelet basis. A Petrov-Galerkin method [LPT91] is used to reduce the determination of the unknown at the new time step to the computation of scalar products. These have to be discretized in an appropriate way. We investigate this point in detail and devise an algorithm that has linear operation count with respect to the number of unknowns. It is tested with spline wavelets and Meyer wavelets retaining the latter for their better localisation at finite precision. The algorithm is then applied to the one dimensional thermodiffusive equations. We show that the adaption strategy merits to be modified in order to take into account the particular and very strong nonlinearity of this problem. Finally, a supplementary Fourier discretization permits the computation of two dimensional flame fronts.

1 Introduction

When numerically solving partial differential equations an adequate spatial resolution is decisive. Hence, a current approach to set up efficient, precise, and robust methods is the construction of self-adaptive discretization procedures that automatically increase the spatial resolution where this is required, such as for example in boundary layer type regions where the solution exhibits steep gradients. Such a method has to contain the following three essential parts:
a) error estimation for the actual approximate solution
b) refinement procedure
c) efficient solution algorithm with non-uniform spatial discretization
We shall describe here such an unsteady, adaptive algorithm using a wavelet discretization in space based on the method of [LT90], [LPT91] further extended in [BMP91]. We will demonstrate that this approach is ideal for the first two of the above tasks. Concerning the third one we describe attempts to devise an efficient solution procedure but it will become clear that this point still diserves further improvements.

Wavelets emerged in signal processing during the early 80s and have soon attracted much attention. It should however be noted that ideas of this type have appeared before as e.g. in the work of Haar, Gabor, Calderon etc. [Me90a]. In the classical discrete case these functions constitute a smooth orthonormal basis posessing a hierarchy in scale and translational invariance. Their properties lead to simple and efficient high compression algorithms for signals and images by an adapted choice of the relevant amplitudes [DJL], [ABMD92] and others. This compression property is very advantageous in order to reduce the degrees of freedom in a numerical algorithm, and in the present paper we will follow this direction.
Let us mention that a slightly different and complementary approach to using wavelets for the numerical solution of PDEs is based on the observation that differential operators are approximately diagonalized when transforming to the description in such a basis [BCR91], [JL92] leading to efficient preconditioners for iterative methods with regular space discretization [DK92], [LL93]. This approch is centered on the operator whereas the former is centered on the actual solution.
Despite the cited attempts and many others, wavelet methods with the above objective are still in their infancy since although appealing from principal, a lot of technical difficulties have yet to be overcome. The two central questions to be adressed are how to introduce boundary conditions and how to cope with nonlinear terms. In our study we will focus on the second of these and describe an adaptive algorithm for a combustion problem. This kind of phenomena is known to develop very pronounced internal layers, the flames, due to the extremly strong nonlinearity of the reaction term. Their characteristic length, i.e. their thickness, is orders of magnitudes smaller than other lenght scales of the problem. This requires thorough spatial discretisation and error control when numerically solving these equations.
We start with introducing equations and geometry together with a transformation that leads to an initial value problem with periodicity of the solution in space. After recalling some required notation, the sections 4 and 5 are devoted to a detailed discussion of the one dimensional algorithm. It is applied to the combustion problem in section 6. Finally,

the algorithm for the two dimensional case is described and illustrated by related numerical results.

2 Equations and geometry

Research on combustion phenomena is characterized by a large number of models that aim to make this generally very complex situation tractable for analytical and numerical investigation, e.g. [Wi85]. The thermodiffusive equations are one of the simplest as they only take into account the diffusive transport of heat and species and the reaction term:

$$\begin{aligned} \partial_t T - \quad \nabla^2 T &= \omega \\ \partial_t Y - \frac{1}{Le}\nabla^2 Y &= -\omega \\ \omega &= \frac{\beta^2}{2Le} Y \exp\left(\frac{\beta(T-1)}{1+\alpha(T-1)}\right) \end{aligned} \tag{1}$$

where T and Y stand for the non dimensional reduced temperature $T = (\bar{T} - \bar{T}_u)/(\bar{T}_b - \bar{T}_u)$ and species concentration, respectively, both attaining values between zero and one. The Arrhenius term for the reaction rate ω contains the dimensionless activation energy β (Zeldovic number), as well as the temperature ratio $\alpha = (\bar{T}_b - \bar{T}_u)/\bar{T}_b$, and resides on an additional approximation for large β [BF70]. The overbar denotes dimensional quantities whereas the indices b and u refer to the burnt and unburnt state, respectively. All our calculations have been performed with $\beta = 10$ and $\alpha = 0.8$.
The problem that we will study is the one of a two dimensional flame front propagating in a pre-mixed atmosphere in positive x-direction. The physical domain is $\Omega = \mathbb{R} \times [-L_y, L_y]$ with boundary conditions

$$\begin{aligned} T(-\infty, y, t) &= 1 \qquad T(\infty, y, t) = 0 \\ Y(-\infty, y, t) &= 0 \qquad Y(\infty, y, t) = 1 \end{aligned} \tag{2}$$

We restrict ourselves here to solutions that are periodic in y-direction, i.e.

$$\begin{aligned} T(x, -L_y, t) &= T(x, L_y, t) \\ Y(x, -L_y, t) &= Y(x, L_y, t) \end{aligned} \tag{3}$$

In the one dimensional case it is possible to determine analytically a steady solution of (1), (2) when considering the limit $\beta \to \infty$, i.e. the high activation energy limit. The non dimensional solution then is

$$\begin{aligned} T_\infty(x) &= \begin{cases} \exp(x-t) & , x \le t \\ 1 & , x > t \end{cases} \\ Y_\infty(x) &= \begin{cases} 1 - \exp(Le(x-t)) & , x \le t \\ 0 & , x > t \end{cases} \end{aligned} \tag{4}$$

travelling with speed one from right to left. For finite β, (4) is altered, and the general expression for the flame speed reads

$$v_f = \frac{1}{2L_y} \int_\Omega \omega(x,y)\, dx\, dy \tag{5}$$

The functions (4) have been used as initial condition in our computations. For the two dimensional cases it has been perturbed sinusoidally in y-direction. The Lewis number Le and the lenght L_y have been chosen in such a way that the plane flame is unstable and develops the well known thermodiffusive instability. The hypothesis (3) of periodicity in y then is justified by the periodicity of the physical solution near criticality and facilitates the numerical procedure.

Using (5) to define a reference frame that follows the propagation of the flame leads to an integro-differential system (its coordinate will still be denoted x).

In [BL88] existence and uniqueness of a solution for the latter formulation are proven as well as for the original formulation (1),(2) with homogeneous Neumann boundary conditions. This carries over to the y-periodic case.

Since for physical reasons T is essentially constant in front of the flame and behind it, the ansatz of a decomposition into a smooth step $S(x)$ plus a perturbation $\tilde{T}(x,y,t)$ is reasonable, i.e. $T = \tilde{T} + S$ and similarly $Y = \tilde{Y} + 1 - S$ leading to

$$\begin{aligned} \partial_t \tilde{T} + v_f \partial_x \tilde{T} - \quad \nabla^2 \tilde{T} &= \quad \tilde{\omega} + \quad d_{xx} S - v_f d_x S \\ \partial_t \tilde{Y} + v_f \partial_x \tilde{Y} - \frac{1}{Le} \nabla^2 \tilde{Y} &= -\tilde{\omega} - \frac{1}{Le} d_{xx} S + v_f d_x S \\ \tilde{\omega} &= \omega(\tilde{T} + S, \tilde{Y} + 1 - S) \end{aligned} \tag{6}$$

with v_f from eq. (5) and ω from (1). [DH90] take

$$S(x) = \frac{1}{2}(1 + \tanh(\tau \tan(\frac{z-\pi}{2}))) \quad ; \quad z = \frac{(x+L_x)\pi}{L_x} \tag{7}$$

All its derivatives vanish at $x = \pm L_x$, and τ determines the slope at the origin (here $\tau = 5$ mostly). One can now choose locations $x = \pm L_x$ far away from the flame and observes that the perturbations as well as all their derivatives become very small. Hence, $\tilde{T}$ and $\tilde{Y}$ can be well approximated by a periodic function in x [DH90].

The boundary conditions in x are thus replaced by the condition of periodicity for the perturbations $\tilde{T}$ and $\tilde{Y}$ so that these become periodic in x and y. We like to avoid the missleading terminology of "periodic boundary conditions" as in fact one solves a pure initial value problem instead of a boundary value problem now.

3 Periodic orthonormal wavelet bases

3.1 Multiresolution in $L^2(\mathbb{R})$

Let us recall some essential features of wavelet approximation in $L^2(\mathbb{R})$ that will be important in the sequel refering to [Me90], [D92], [C92] for an exhaustive treatment. The discrete wavelet transform resides on the concept of multiresolution [Ma89], [Me89] which is a sequence of imbedded subspaces V_j with - in the case of $L^2(\mathbb{R})$

$$V_j \subset V_{j+1} \qquad \forall j \in \mathbb{Z} \tag{8}$$

$$\overline{\bigcup}_{j\in\mathbb{Z}} V_j = L^2(\mathbb{R}) \tag{9}$$

$$\bigcap_{j\in\mathbb{Z}} V_j = \{0\} \tag{10}$$

$$f(x) \in V_j \Leftrightarrow f(2x) \in V_{j+1} \tag{11}$$

A scaling function $\phi(x)$ is required to exist of which the translates generate a basis in each V_j, via

$$V_j = \overline{span}\{\phi_{ji}\}_{i\in\mathbb{Z}} \tag{12}$$

with

$$\phi_{ji}(x) = 2^{j/2}\phi(2^j x - i) \qquad j,i \in \mathbb{Z} \tag{13}$$

In the classical case this basis is orthonormal, so that

$$< \phi_{ji}, \phi_{jk} >_{\mathbb{R}} = \delta_{ik} \tag{14}$$

with $< f,g >_{\mathbb{R}} = \int_{-\infty}^{+\infty} f(x)\overline{g}(x)\,dx$ being the usual $L^2(\mathbb{R})$ inner product. The main issue of the wavelet approach now is to work with the orthogonal complement spaces W_j defined by

$$V_{j+1} = V_j \oplus W_j \tag{15}$$

Based on the function $\phi(x)$ one can find a function $\psi(x)$, the so-called mother wavelet, of which the translates and dilates constitute orthonormal bases of the spaces W_j.

$$W_j = \overline{span}\{\psi_{ji}\}_{i\in\mathbb{Z}} \tag{16}$$

generated by the wavelets

$$\psi_{ji}(x) = 2^{j/2}\psi(2^j x - i) \qquad j,i \in \mathbb{Z} \tag{17}$$

Each function $f \in L^2(\mathbb{R})$ can now be expressed as

$$f(x) = \sum_{i\in\mathbb{Z}} c_{j_0 i}\,\phi_{j_0 i}(x) + \sum_{j=j_0}^{\infty}\sum_{i\in\mathbb{Z}} d_{ji}\,\psi_{ji}(x) \tag{18}$$

where

$$c_{ji} = < f, \phi_{ji} >_{\mathbb{R}} \qquad d_{ji} = < f, \psi_{ji} >_{\mathbb{R}} \tag{19}$$

Of course, in numerical applications the sums in (18) are truncated which corresponds to the projection of f into a subspace of $V_J \subset L^2(\mathbb{R})$. The decomposition (18) is orthogonal, as, by construction,

$$< \psi_{ji}, \psi_{lk} >_{\mathbb{R}} = \delta_{jl}\ \delta_{ik} \tag{20}$$

$$< \psi_{ji}, \phi_{lk} >_{\mathbb{R}} = 0 \qquad j \geq l \tag{21}$$

in addition to (14).

3.2 Regularity and local decay of wavelet coefficients

It is well known that the local or global regularity of a function is closely related to the decay of its wavelet coefficients. The latter directly determines the error being made when truncating a wavelet sum at some scale. Depending on the type of norm and wether global or local characterisation is concerned, various relations of this kind have been developed. See [Me90], [D92], [JL92] for an overview. Let us recall here only briefly as an example the case of an α-Lipschitz function [HT89], taken from [BMP91] which is generalized to $\alpha \geq 1$ and discussed in some detail in [MaHw92].

Suppose $f \in L^2(\mathbb{R})$, then for $[a,b] \subset \mathbb{R}$ the function f is α-Lipschitz for any $x_0 \in [a,b]$, i.e. $|f(x) - f(x_0)| \leq C|h|^\alpha$, if and only if there exists a constant A such that $| < f, \psi_{ji} > | \leq A 2^{-j\alpha - \frac{1}{2}}$ for any (j,i) with $\frac{i}{2^j} \in]a,b[$.

This shows the relation between the local regularity of a function and the decay of its wavelet coefficients in scale. The adaptive discretization discussed in this paper is precisely based on taking into account spatially varying regularity of the solution through a variable cut off in scale of its wavelet series.

3.3 Periodic multiresolution

Following [PB89], [Me90] we now construct a multiresolution of $L^2(\mathbb{T})$, i.e. of 1-periodic functions living on the torus $\mathbb{T} = \mathbb{R}/\mathbb{Z}$. The key point is to map a function $f \in L^2(\mathbb{R})$ onto a function $\tilde{f} \in L^2(\mathbb{T})$ by the relation

$$\tilde{f}(x) = \sum_{n \in \mathbb{Z}} f(x+n) \tag{22}$$

(the tilde will always denote periodicity in this section). In Fourier space this relation reads

$$\hat{\tilde{f}}_k = \hat{f}(k) \qquad k \in \mathbb{Z} \tag{23}$$

where

$$\hat{f}(\omega) = \int_{-\infty}^{+\infty} f(x)\ \exp(-2\pi i\omega x)\, dx \tag{24}$$

defines the continuous Fourier transform in $L^2(\mathbb{R}) \cap L^1(\mathbb{R})$ and

$$\hat{\tilde{f}}_k = \int_0^1 \tilde{f}(x)\ \exp(-2\pi ikx)\, dx \tag{25}$$

the Fourier transform in $L^2(\mathbb{T})$. Applying this technique to ϕ_{ji} and ψ_{ji} one obtains [PB89]

$$\tilde{V}_j = \{\tilde{f} \mid \tilde{f}(x) = \sum_{i=0}^{2^j-1} c_{ji}\, \tilde{\phi}_{ji}(x)\} \qquad j \geq 0 \tag{26}$$

$$\tilde{W}_j = \{\tilde{f} \mid \tilde{f}(x) = \sum_{i=0}^{2^j-1} d_{ji}\, \tilde{\psi}_{ji}(x)\} \qquad j \geq 0 \tag{27}$$

where $j \geq 0$, since $\tilde{V}_j$ contains the constant functions and $\tilde{W}_j = \{0\}$ for $j < 0$.
The definition of a multiresolution in the periodic case carries over with only slight technical modifications from the nonperiodic one described above [PB89].

For the wavelet transform, a function $\tilde{f}(x) \in L^2(\mathbb{T})$ is projected onto $\tilde{V}_J$ and decomposed into contributions from $\tilde{V}_0$ and $\tilde{W}_j, (j = 0, \ldots, J-1)$. For conciseness we set

$$\tilde{\psi}_{-10} = \tilde{\phi}_{00} \qquad\qquad d_{-10} = c_{00} \tag{28}$$

$$A_J = \{\,(j,i) | -1 \leq j < J\,,\, 0 \leq i < 2^j\,\} \tag{29}$$

and write

$$\tilde{f}_J(x) = \sum_{(j,i)\in A_J} d_{ji}\ \tilde{\psi}_{ji}(x) \tag{30}$$

with

$$d_{ji} = < \tilde{f}, \tilde{\psi}_{ji} >_{\mathbb{T}} \tag{31}$$

The decomposition (30) is orthogonal, since, by construction, the orthogonality carries over from (18) to the torus with

$$< \tilde{f}, \tilde{g} >_{\mathbb{T}} = \int_0^1 \tilde{f}(x)\bar{\tilde{g}}(x)dx \tag{32}$$

Note, that in contrast to the nonperiodic case (18) the sums over i in (26), (27) and (30) do not spread all over $\mathbb{Z}$ and that there is a minimal j, namely $j_0 = 0$. Regularity relations carry over from the non periodic case without change.
In the present study we apply real valued periodic spline wavelets of even order m or Meyer wavelets and refer to the Appendices for their expressions. The subscript $\mathbb{T}$ and the tilde for functions and spaces derived from a periodic multiresolution will be dropped for simplicity.

4 The one dimensional algorithm

The evolution equations in (6) have the form

$$\begin{aligned} \partial_t u + L(u) - F(u) - \partial_x G(u) &= 0 \quad ; \qquad \text{for } x \in [0,1]\,,\ t > 0 && (33)\\ u(0,t) &= u(1,t) && (34)\\ u(x,t=0) &= u_0(x) && (35) \end{aligned}$$

with L being the leading linear differential operator in space and F and G (generally nonlinear) functions of u. They read for the temperature equation

$$\begin{aligned} L(\tilde{T}) &= -\nabla^2 \tilde{T} && (36)\\ F(\tilde{T}) &= \bar{\omega}(\tilde{T},\tilde{Y}) + d_{xx}S - v_f d_x S && (37)\\ \partial_x G(\tilde{T}) &= -v_f \partial_x \tilde{T} && (38) \end{aligned}$$

Up to signs and the Lewis number the above also holds for the equation of the concentration. In this chapter we concentrate on the one dimensional case setting $L = -\partial_{xx}$.

4.1 Discretization in time

Equation (33) is discretised in time by a finite difference scheme of mixed type. A semi-implicit two-step scheme, avoids the solution of nonlinear equations by an explicit scheme for these terms. On the other hand the restrictive stability condition of a pure explicit scheme is eleminated by discretizing the linear terms $L(u)$ with an implicit scheme. We use a backward scheme of 2nd order, combinded with the second order extrapolation $F^{n,n-1}(u) = F(2u^n - u^{n-1})$. Due to the strong nonlinearity, we experienced slightly better precision when using the latter instead of the classical Adams-Bashforth-scheme of second order. We use

$$\sigma u^{n+1} + L(u^{n+1}) = \frac{4}{3}\sigma u^n - \frac{1}{3}\sigma u^{n-1} + F^{n,n-1} + \partial_x G^{n,n-1} \qquad (39)$$

with the time step Δt, $t^n = n\Delta t$, and $\sigma = 3/(2\Delta t)$. A suitable first order scheme is employed for start up.

4.2 Spatial discretization

In this section we recall the method of [LT90] which is discussed in [T89] from a mathematical point of view. It uses in a particular way the classical method of weighted residuals [F72] (also termed Petrov-Galerkin method) which is based on the definition of a space of trial functions X_N and space of testfunctions Y_N. Both spaces are N-dimensional subspaces of a Hilbert space, here $L^2(I\!I)$. The minimisation of the weighted residual of (39) supplied with the initial condition requires for $u^n \in X_N$ that

$$< (\sigma + L)u^{n+1} - \frac{4}{3}\sigma u^n + \frac{1}{3}\sigma u^{n-1} - F^{n,n-1} - \partial_x G^{n,n-1} , v >= 0 \quad ; \quad \forall v \in Y_N \quad (40)$$

$$< u^0, v >=< u_0, v > \quad ; \quad \forall v \in Y_N \quad (41)$$

In our case, the trial space is spanned by the wavelets of chapter 3, i.e. $X_N = V_J$ with $N = 2^J$ so that the unknown u^n is approximated by

$$u^n(x) = \sum_{(j,i)\in A_J} d_{ji}^n \, \psi_{ji}(x) \quad (42)$$

The testfunctions are chosen in such a way that the Galerkin matrix turns out to be the identity [LT90]. This is achieved with, formally,

$$\begin{aligned} \theta_{ji} &= ((\sigma + L)^{-1})^* \psi_{ji}(x) \qquad ; (j,i) \in A_J \setminus \{(-1,0)\} \quad (43) \\ \theta_{-1,0} &= \sigma^{-1} \phi_{0,0} \end{aligned}$$

(using * to indicate the adjoint) and

$$Y_N = span\{\theta_{ji}\}_{(j,i)\in A_J} \subset L^2(I\!T) \quad (44)$$

In the present case it is possible to determine the testfunctions in Fourier space by

$$(\widehat{\theta_{ji}})_k = \frac{1}{\sigma + 4\pi^2 k^2} (\widehat{\psi_{ji}})_k \qquad ; k \in Z\!\!\!Z \quad (45)$$

Thanks to periodicity,

$$< \partial_x G_N^{n,n-1}, \theta_{ji} >= - < G_N^{n,n-1}, \theta'_{ji} > \quad (46)$$

which amounts just to use different test functions for this term.
Let us recall that due to the nonhomogenity of the differential operator no rescaling property for θ_{ji} and θ'_{ji} holds. Translation invariance and localisation in the frequency and physical space are preserved.

The discrete equation for the function u^{n+1} finally writes

$$< u^{n+1}, \psi_{ji} > = < \frac{4}{3}\sigma u^n - \frac{1}{3}\sigma u^{n-1} + F^{n,n-1}, \theta_{ji} > - < G^{n,n-1}, \theta'_{ji} > \quad (47)$$

reducing the solution of the Petrov-Galerkin equations to the calculation of appropriate scalar products. This avoids the inversion of a linear system as in [MPR92] which has the disadvantage that the stiffness matrix changes whenever the grid is modified by adaption. Figure 1 shows the graph of the functions ϕ, ψ, θ and μ with

$$\mu_{ji} = (\sigma - \partial_{xx})\psi_{ji} \quad (48)$$

for the spline multiresolution with $m = 6$ in physical space and in Fourier space (in fact the latter are the Fourier coefficients for $k = 0, ..., 256$ connected by lines).

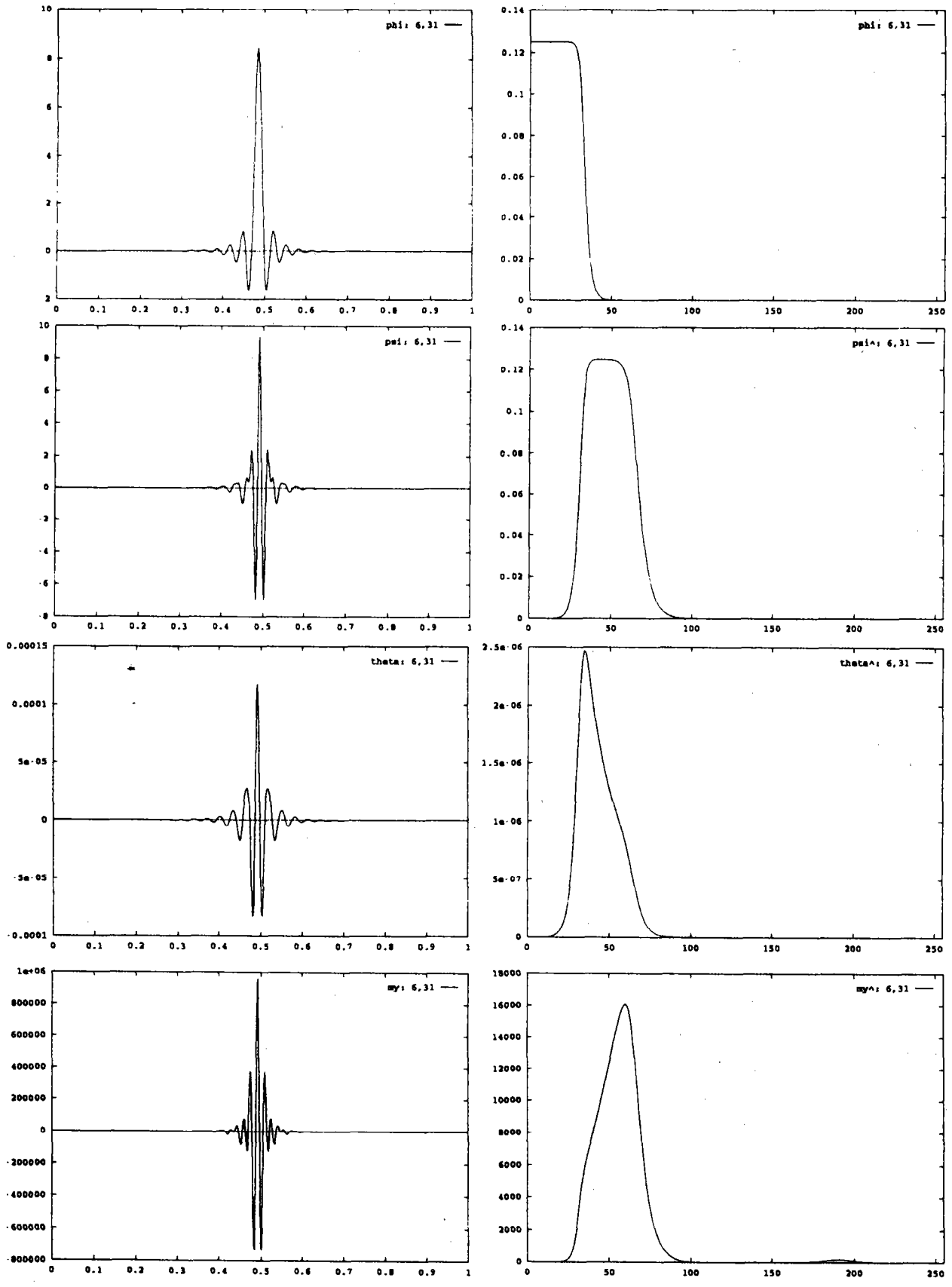

Figure 1: The functions ϕ, ψ, θ and μ in physical and Fourier space.

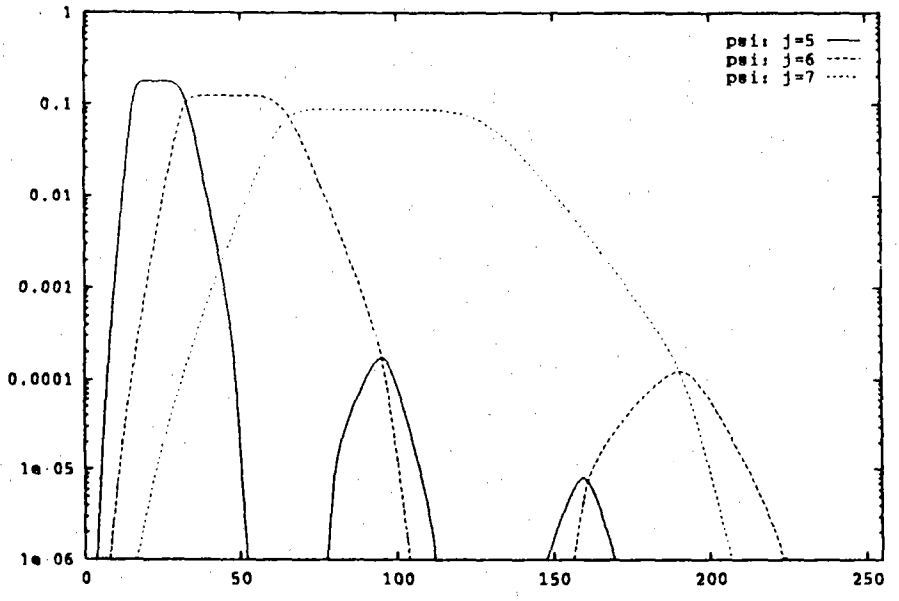

Figure 2: Spline wavelets $|(\widehat{\psi}_{ji})_k|$ for j= 5,6,7 in logarithmic scale.

To illustrate further discussion we add Figure 2 showing $|(\widehat{\psi}_{ji})_k|$ for different j in logarithmic scale. The "bumps" originate from the finite regularity of the spline spaces.
They are enhanced by derivation as e.g. for μ (Figure 1). For Meyer wavelets the plots corresponding to Figure 1 look very similar so that they are omitted here. A relevant difference is the compact support which is illustrated by Figure 3 plotted with the same parameters as Figure 2.

4.3 Adaptive discretization

Discretizing the solution of a PDE using a wavelet basis in space is perticulary attractive due to the ease with which a strategy for adaption can be devised. The following procedure [LT90] [MPR91] is the result of wedding the vortex method type idea of mobile wavelets [BHP90] that directly considers the evolution in scale space with wavelet compression as used in signal processing. Consider the ϵ -representation u_ϵ of u determined by cancelling all wavelet coefficients having absolute value below ϵ . The results on the convergence of wavelet series to smooth functions allow to state that the error $u - u_\epsilon$ measured in the L^2 norm or in a Sobolev norm is asymptotically of order ϵ , similar to spectral methods [CHQZ88] (c.f. section 3.2). Assume now J being sufficiently large to get $(u_J)_\epsilon = u_\epsilon$. Then the elimination of coefficients below ϵ leads to an index set $A_J(u,\epsilon)$ that defines the corresponding subspaces X_N and Y_N. To account for the evolution of indices from one time step to another the set $A_J(u,\epsilon+)$ is used which comprises $A_J(u,\epsilon)$ and the neighbours of each index. The definition

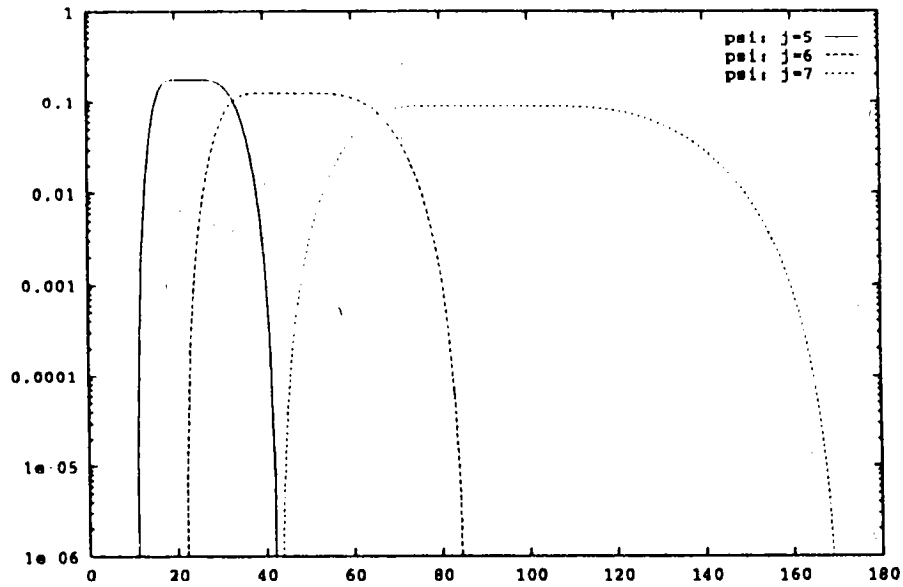

Figure 3: Meyer wavelets $|(\widehat{\psi}_{ji})_k|$ for j= 5,6,7 in logarithmic scale.

of how far this neighbourhood actually reaches depends on the problem and the size of the time step. We choose the adjacent ones as depicted in Figure 4.

After initialisation each time step consists of three parts

Index set Determine $A_J(u^n, \epsilon)$, $A^{n+1} = A_J(u^n, \epsilon+)$ and therewith X^{n+1}, Y^{n+1}

right hand side Determine the right hand side in physical space using the corresponding index sets A^n and A^{n-1} for u^n, and u^{n-1}, respectively, on some grid in physical space.

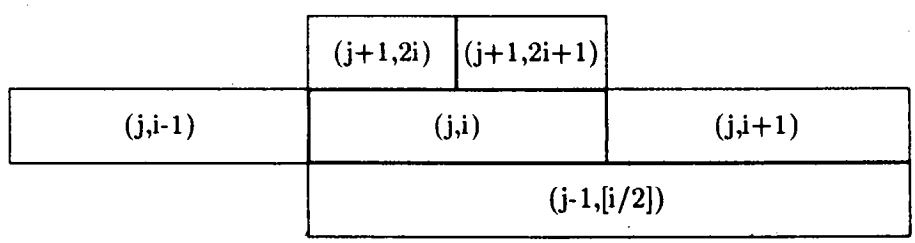

Figure 4: Neighbourhood of a coefficient d_{ji} in scale space.

This grid is choosen such that it permits to integrate for the coefficients determined by A^{n+1}.

Solution Compute d_{ji}^{n+1} for $(j,i) \in A^{n+1}$. Note that there are no coefficients "lost" or set to zero when changing test and trial space.

The present equations involve two unknowns, $\tilde{T}$ and $\tilde{Y}$. We took the same index set $A^{n+1} = A_J(\tilde{T}, \epsilon+) \cup A_J(\tilde{Y}, \epsilon+)$ for both equations.
For some applications it might be usefull to generalize the criteria for A^{n+1} in one of the following ways
- different index sets for different unknowns (here $\tilde{T}$ and $\tilde{Y}$).
- different precisions ϵ_T and ϵ_Y for $\tilde{T}$ and $\tilde{Y}$, respectively.
- ϵ varying in space: $\epsilon = \epsilon(x)$, or ϵ depending on scale and space: $\epsilon = \epsilon(j,i)$.
- extrapolation of type $(A^{n-1}, A^n) \rightarrow A^{n+1}$.

We will come back to this point in section 6.2.

4.4 Evaluation of the right hand side

In order to determine the non-linear right hand term $F^{n,n-1}$ it would be ideal to stay in coefficient space, i.e. to calculate with the wavelet coefficients of $\tilde{T}$ and $\tilde{Y}$ directly. This however is impossible for several reasons. In [BCR91] a wavelet procedure for the fast multiplication of matrices is devised. If a non linear operator can be well approximated by a series of products (such as the term u^2 in Burgers equation) this technique may lead to efficient computations in some cases [JL92]. Since it requires the coefficients c_{ji} of the scaling function, the "non-standard form" which is applied is not efficient in the case of adaptive discretization [Ch93]. The use of the "standard form" requiring only the coefficients d_{ji} would however be possible. For the present expression $\tilde{\omega} = \tilde{\omega}(\tilde{T}, \tilde{Y})$ the periodisation technique complicates the situation. Furthermore, a Taylor series of the exponential term converges very slowly, so that the approximation by products would be bad. We therefore evaluated $F^{n,n-1}$ and $G^{n,n-1}$ in physical space on a suitable set of grid points. The subsequent calculation of the scalar products to solve (47) is discussed in detail in the next section.

5 Computation of the required scalar products

5.1 The regular wavelet transform for periodic functions

As a starting point we recall the transformation described in [PB89] and take the occasion to indicate a computational trick for its acceleration. In case of a regular discretization and periodic functions computations can be done in physical space by periodizing the required filters. For long filters it is more economical, however, to use fast convolution in Fourier space employing FFT. The algorithm then reads

0. step FFT of the values $\{f_i\}_{i=0,\ldots,2^J-1}$ at the points $\{x_i = \frac{i}{2^J}\}_{i=0,\ldots,2^J-1}$ to the Fourier coefficients $\{\hat{f}_k\}_{k=0,\ldots,2^J-1}$.

1. step Interpolation using the Lagrange function $S_J(x)$ of the space V_J (such a function always exists [Wa92]) by computation in Fourier space.

2. step Application of Filters g and h in Fourier space

$$(\widehat{c^*_{J-1}})_k = \overline{\hat{h}_k}\,(\widehat{c_J})_k \qquad k = 0,\ldots,2^J-1 \tag{49}$$

$$(\widehat{d^*_{J-1}})_k = \overline{\hat{g}_k}\,(\widehat{c_J})_k \qquad k = 0,\ldots,2^J-1 \tag{50}$$

3. step Instead of setting

$$c_{J-1,i} = c^*_{J-1,2i} \qquad d_{J-1,i} = d^*_{J-1,2i} \qquad i = 0,\ldots,2^{J-1}-1 \tag{51}$$

in physical space, downsampling can be done directly in Fourier space through

$$(\widehat{c_{J-1}})_k = (\widehat{c^*_{J-1}})_k + (\widehat{c^*_{J-1}})_{k+2^{J-1}} \qquad k = 0,\ldots,2^{J-1} \tag{52}$$

$$(\widehat{d_{J-1}})_k = (\widehat{d^*_{J-1}})_k + (\widehat{d^*_{J-1}})_{k+2^{J-1}} \qquad k = 0,\ldots,2^{J-1} \tag{53}$$

4. step Inverse FFT of lenght 2^{J-1} to get $\{d_{J-1,i}\}_{i=0,\ldots,2^{J-1}-1}$

iterate steps 2 to 4 down to $j = 0$

The use of (52), (53) instead of (51) leads to a speed up by a factor of 6 with respect to extraction of coefficients in physical space. The inverse transform is obtained by executing the above steps in reversed order omitting the conjugate complex in (49), (50) and replacing step 3 with upsampling in Fourier space.
Remark: As in (51), a comma will be inserted between the indices without deeper meaning whenever suitable for readability.

5.2 Scalar products on a regular grid

For the purpose of calculating the scalar products $d_{ji} = < f, \theta_{ji} >$ with a regular discretization [LT90] divise the following hierarchical algorithm. (Application of all filters and downsampling can be carried out in Fourier space as in section 5.1.)

1. step Interpolate the values f_i of the function $f(x)$ at the grid points $\{x_i = i/2^J\}_{i=0,\ldots,2^J-1}$ by $f_J(x) = \sum_i c_{J,i}\,\phi_{J,i}(x)$

2. step Apply the filter $\{\alpha_{J,i}\}_{i=0,\ldots,2^J-1} = \{< \phi_{J,i}\,,\, \theta_{J-1,0} >\}_{i=0,\ldots,2^J-1}$ to get the amplitudes $d_{J-1,i}$ of u.

3. step Compute $\{c_{J-1,i}\}_{i=0,\ldots,2^{J-1}-1}$ and $\{d_{J-1,i}\}_{i=0,\ldots,2^{J-1}-1}$ of f in the usual way using the filters h and g, respectively.

4. step Apply the filters $\{\alpha_{J-1,i}\}_{i=0,\dots,2^{J-1}-1}$ and $\{\beta_{J-1,i}\}_{i=0,\dots,2^{J-1}-1} = \{< \psi_{J-1,i}, \theta_{J-2,0} >\}_{i=0,\dots,2^{J-1}-1}$ to the $\{c_{J-1,i}\}$ and $\{d_{J-1,i}\}$, respectively, then adding both contributions to get $\{d_{J-2,i}\}_{i=0,\dots,2^{J-2}-1}$ of u.

iterate steps 3 and 4 down to $j = 0$.

The above procedure resembles the non-standard form of an operator in [BCR91] with an additional approximation. It relies on the bandpass-type spectrum of the function ψ, $(\hat{\psi}_{ji})_k$ being essentially supported on $|k| \in [2^{j-1}, 2^{j+1}]$. This carries over to θ and μ (c.f. Figures in section 4). Hence,

$$| < \psi_{ji}, \theta_{j-\delta_j,k} > | < \epsilon(\delta_j) \tag{54}$$

with ϵ depending on the difference in scale δ_j and on the type of multiresolution considered. In particular $\epsilon = 0$ for $\delta_j > 1$ in the case of Meyer wavelets as to be seen in Figure 3. Figure 2 nicely illustrates the origine of ϵ in (54) and its decay with δ_j for the spline wavelets.

The above algorithm neglects the terms in (54) as soon as $\delta_j > 1$. This introduces an error of $O(\epsilon)$ in each amplitude and hence an error of $O(J\epsilon)$ in the L^2 norm of the computed solution. For spline wavelets with $m = 6$ we find $\epsilon = O(10^{-3})$ [LT90].
This error can not be corrected by, for instance, adding supplementary basis functions through an adaptive procedure, since these new functions live on entirely different scales. Hence, it persists and determines a sort of basic noise level, adaption with higher precision is impossible. In cases of high precision requirements the value of ϵ in (54) has to be reduced. For spline wavelets this can be done e.g. by increasing the degree of the spline or by introducing a third filter (or even more) which, however, increases computation cost and complexity of the algorithm.
Another aspect is that the above procedure employs a collocation projection of f onto the space $X_N = V_J$ and only subsequently determines the projection based on the functions $\theta_{ji} \in Y_N$. In the asymptotic limit this is of no importance as the error is of the order of the truncation error. When this regular algorithm is extended by locally adding supplementary fine scale basis functions, however, the amplitude for the fine scales of the regular part is no longer small for all of the coefficients. In this case the precision may be degraded by the additional projection.
The computational cost for the above algorithm is $O(N \log N)$ with $N = 2^J$. We like to indicate that the same operation count of $O(N \log N)$ is obtained when, without any recursion or approximation, the products $d_{ji} =< f, \theta_{ji} >$ are directly calculated in Fourier space:

1. step FFT of the values $\{f_i\}_{i=0,\dots,2^J-1}$ to the Fourier coefficients $\{\hat{f}_k\}_{k=0,\dots,2^J-1}$.

2. step Compute $\hat{f}_k \overline{(\widehat{\theta_{J-1,0}})_k}$ for $k = 0, \dots, 2^J - 1$. This is exactly the trapezoidal rule on a grid $2^{jQ} = 2^J$ evaluated by fast correlation.

3. step Determine $\{d_{J-1,i}\}_{i=0,\dots,2^{J-1}-1}$ by downsampling similar to (52) and inverse FFT.

iterate steps 2 and 3 down to $j = -1$.

In step 2 one can conserve the range for k or benefit from localization of $\hat{\theta}$ in frequency space to save multiplications.

With our current implementation we experienced an increase of 10% and a reduction of 20% for the latter method with respect to the recursive procedure when $J = 7$ and $J = 8$, respectively. The result was free from approximation error due to neglecting the terms (54). In the case of spline wavelets the procedure for a regular discretization closely resembles a collocation method with periodic splines, just supplied with a transform to the corresponding wavelet bases. It should be recalled that the recursive procedure has been set up to deal with the adaptive case where this no longer holds. For regular discretization we think it is more convenient to work with the basis

$$\{\phi_{Ji}\}_{i=0,\ldots,2^J-1} \tag{55}$$

When adapting the spatial discretization one will in the present context generally use all basis functions ψ_{ji} in some regular low scale part, i.e. for j smaller than some J_r and a locally refined discretization for $J_r \leq j < J$. In that case it would be advisabel to use the basis

$$\{\phi_{J_r i}\}_{i=0,\ldots,2^{J_r}-1} \bigcup \{\psi_{ji}\}_{i=0,\ldots,2^j-1\,,\,j=J_r,\ldots,J-1} \tag{56}$$

to represent the solution of the PDE. For implementation reasons we kept the pure wavelet basis down to $j = 0$ and applied the non-recursive FFT procedure in the regular part $j < J_r$.

5.3 Quadrature formula

The method described in the preceeding section is applicable only in the case of a regular discretization, i.e. when on a scale j all amplitudes $d_{ji} =< f, \theta_{ji} >$ are to be computed. Of course, if this is so for all scales and during the whole evolution in time, a Fourier discretization is the method of choice in the periodic case due to convergence properties for regular functions and computational efficiency. If, however, the solution develops steep gradients, the number of degrees of freedom can substanitially be reduced by an adaptive discretization, and one has to study the trade off between this reduction and the increasing cost per degree of freedom for a given type of problem.
In the present and the following sections we will discuss an efficient way to compute the required scalar products in physical space (recall the neccessity of evaluating f in physical space mentioned in section 4).

For testing we consider in the sequel the quantities

$$E_{jlk} = < \mu_{j0}\,,\, \theta_{lk} >_Q \; - \delta_{jl}\,\delta_{0k} \tag{57}$$

$$E'_{jlk} = < \partial_x^{-1}\mu_{j0}\,,\, \partial_x\theta_{lk} >_Q \; - \delta_{jl}\,\delta_{0k} \tag{58}$$

where $< .,. >_Q$ signifies the evaluation of the integral by a quadrature rule to be specified. Due to the construction of μ and θ these functions are orthonormal and E and E' are zero

in case of exact evaluation. All computations, exept if stated explicitly, have been performed with single precision in IEEE-754-1990 standard.

The simplest quadrature rule is the trapezoidal rule and will be used throughoutly. It reads, applied on a grid j_Q for the d_{ji},

$$< f , \theta_{ji} >_Q = \frac{1}{2^{jQ}} \sum_{k=0}^{2^{jQ}-1} f(\frac{k}{2^{jQ}}) \theta_{ji}(\frac{k}{2^{jQ}}) \tag{59}$$

We took this procedure here in order to avoid further intermediate projections. The use of spline quadrature in the case of spline wavelets may be another possibility, but obviously neither $f(x)\theta_{ji}(x)$ nor f, θ or μ are spline functions in that case. For the time being we therefore stick with (59).
The first observation to be made when using (59) is the well known aliasing effect [CHQZ88]. Assume f and θ_{ji} being bandpassed with maximal frequency 2^{J-1}. The product $f\,\theta_{ji}$ then is bandpassed with maximal frequency 2^J. Hence, $j_Q = J+1$ is required in (59) for evaluation, but then the result is exact indeed up to machine error. If the high frequency contributions in both functions have small amplitude the aliasing error can be small leading to satisfactory results even with coarser grid.
Using the whole support and the finest grid $j_Q = J + 1$ for any product the error was max E = 4.2_E-6 (i.e. machine precision) for Meyer wavelets and max E = 3.0 E-3 for spline wavelets (due to undersampling).

5.4 Use localization in frequency space

If for every integral the grid with $j_Q = J + 1$ is used as in the preceeding section, this is very costly. Obviously, it is interesting to use the localization of $\hat{\theta}$ appearing in Figure 1 in order to evaluate the integral on a coarser grid if j is small. However, high frequency components in f would lead to aliasing errors if this being done directly. Loosly speaking one has to substract these parts from f before going to a coarser grid.
Such a procedure resides on the representation of f in terms of $\{\mu_{ji}\}$

$$f = \sum_{ji} < f , \theta_{ji} > \mu_{ji} \tag{60}$$

These functions do not generate a multiresolution as they are not obtained by shift and dilation from one mother-function, but they can be used in a similar way. It can be shown that the spaces M_j spanned by functions of same scale j are included one in each other. Furthermore, in the periodic case being discussed here the functions $\{1/(2^{2j})\,\mu_{ji}\}$ form a Riesz basis of $L^2(\mathbb{T})$. As for numerical purposes j is always bounded we left out the factor and used the μ_{ji} directly. Due to orthonormality then

$$< f , \theta_{ji} > = < f - < f, \theta_{j'i'} > \mu_{j'i'} , \theta_{ji} > \tag{61}$$

for $(j,i) \neq (j',i')$ which leads to the following algorithm:

(K_Q, K_S)	max E	max E'
all points	9.5 E-7	2.4 E-6
(80;60)	1.8 E-5	3.1 E-5
(60;60)	6.1 E-5	3.2 E-5
(50;50)	1.0 E-4	1.3 E-4

Table 1: Error in the numerical orthogonality of θ and μ for truncated quadrature and substraction.

0. step Set $j = J$, and $f^{(j)} = f$.

1. step Determine

$$d_{j-1,i} = < f^{(j)}, \theta_{j-1,i} >_Q \tag{62}$$

with $j_Q = j + 1$ for all required i.

2. step Substract

$$f^{(j-1)} = f^{(j)} - \sum_i d_{j-1,i}\, \mu_{j-1,i} \tag{63}$$

for the values of i considered in (62).

iterate steps 1 and 2 for j down to J_r.

regular part For $j = J_r$ down to $j = -1$ use the FFT procedure of section 5.2.

The variable step size 2^{-j_Q} of the quadrature is essential. Consider wavelets with compact support in frequency space as the Meyer wavelets. The functions θ and μ enherit the bandpass-type spectrum (c.f. Figure 1) so that the procedure starts with the finest grid for the determination of the $d_{J-1,i}$ subsequently substracting the corresponding components in f. The updated function $f^{(J-1)}$ then no longer contains high frequency contibutions so that the integration for the next lower level may be performed on a grid which is twice as large. The first row of Table 1 reports on the corresponding test for Meyer wavelets, the result is of machine error.

Spline wavelets do not have compact support in frequency space, although the decay of the spectrum becomes relatively fast for large degree m, i.e. high regularity in space. Hence the arguments from above only hold approximatively. The precision available at most is determined by the result of max E = 3.0 E-3 of the previous section. In particular when considerable energy is contained in fine scale amplitudes error propagation leads to insufficient numerical precision in some applications (see also following section).

Note that with the present successive coarsening of the quadrature we employ an approximation in physical space which is similar to neglecting the terms in (54). It avoids, however, the determination of the wavelet amplitudes of f as intermediate step.

5.5 Use localization in physical space

The next step is to take advantage of the decay of θ and μ in physical space for accelerating the computations. We therefore replace the functions ψ, θ, μ and so on by functions cut off at a distance R from their center defining e.g.

$$\psi_{ji}^R(x) = \psi_{ji}(x)\, \chi_{[\frac{2i+1}{2j+1}-R, \frac{2i+1}{2j+1}+R]} \tag{64}$$

The related errors of $\|\psi_{ji}^R - \psi_{ji}\|$ in the L^∞ and L^2 norm as a function of R are plotted in Figure 5 and 6, respectively, computations being done in double precision.
It is well known that spline wavelets have exponential decay in space. The Meyer wavelets have a decay that depends on the regularity of their Fourier transform, i.e. on the function $\nu(\omega)$ appearing in the construction (c.f. Appendix B). This, however, does only determine the asymptotic behaviour. The plots in Figure 5 exhibit this behaviour, but they show as well that for moderate precision the numerical support of the Meyer wavelets, at least the ones we used, is smaller than the support of the spline wavelets.
The curves in Figure 6 are particularly interesting as they compare the L^2-error for given truncation R. Down to a fairly low error the Meyer wavelets require smaller numerical support than the spline wavelets with $m = 6$ (for $m = 4$ their decay is somewhat stronger,of course). Furthermore, an interesting numerical effect is to be observed. The L^2-error had to be computed numerically using a particular grid. As soon as $j_Q \geq j + 2$ all frequency components of the Meyer wavelets ψ_{ji} are captured and machine accurancy is achieved. For spline wavelets in contrast, coarse grids prevent from correctly sampling the high frequency components visible in Figure 2. The locking of precision at some level directly monitors the effect of using a particular grid for quadrature and subtraction. (The effect is enhanced for $m = 4$ and smaller for $m > 6$.)

We can now complete the algorithm for the approximate computation of the required scalar products by restricting the quadrature and the substraction to a region around the center of θ_{ji} and μ_{ji}, respectively. This region scales with j and leads together with the successive sparcening described in the previous section to a constant number of grid points involved for each scalar product. Therefore, thanks to the localization in frequency and space, the procedure is linear in the number of retained coefficients d_{ji} in (42).

5.6 Convergence

In each time step an elliptic problem is solved by the method described so far. We now investigate the convergence of the spatial approximation of the solution to the exact one in the following model problem:

$$\sigma u - \partial_{xx} u = f \tag{65}$$

with exact solution

$$u_{ex} = \exp(-\gamma^2 (x - \frac{1}{2})^2) \tag{66}$$

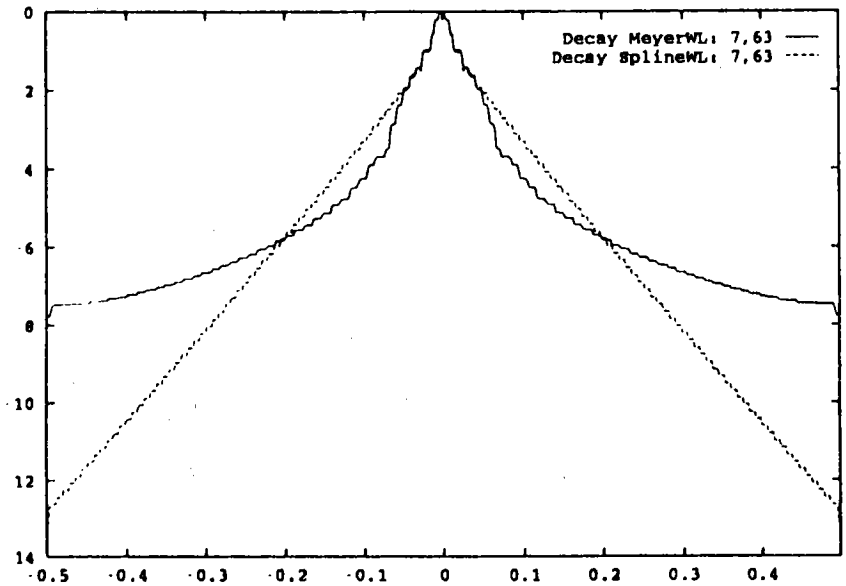

Figure 5: $\|\psi_{ji}^R - \psi_{ji}\|_\infty$ for spline wavelets ($m = 6$) and Meyer wavelets in logarithmic scale.

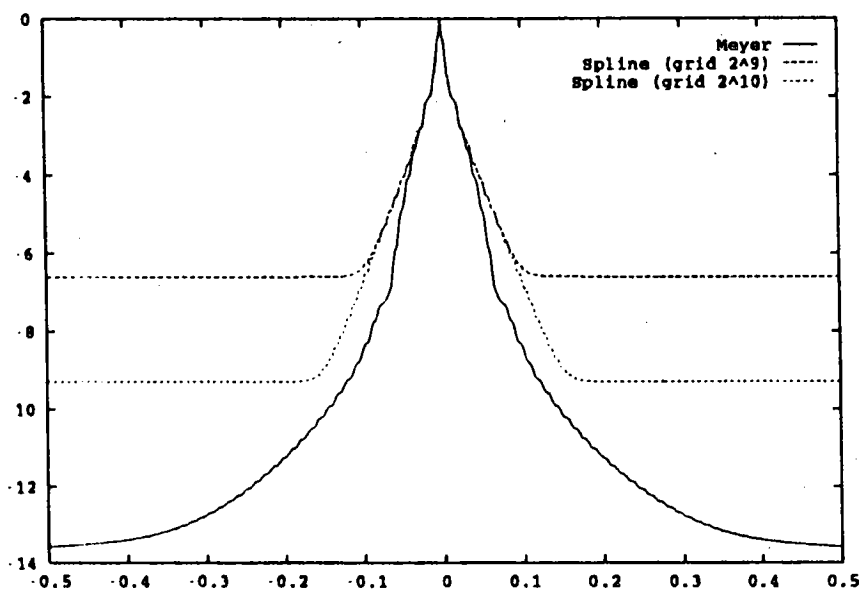

Figure 6: $\|\psi_{ji}^R - \psi_{ji}\|_2$ for spline wavelets ($m = 6$) and Meyer wavelets in logarithmic scale.

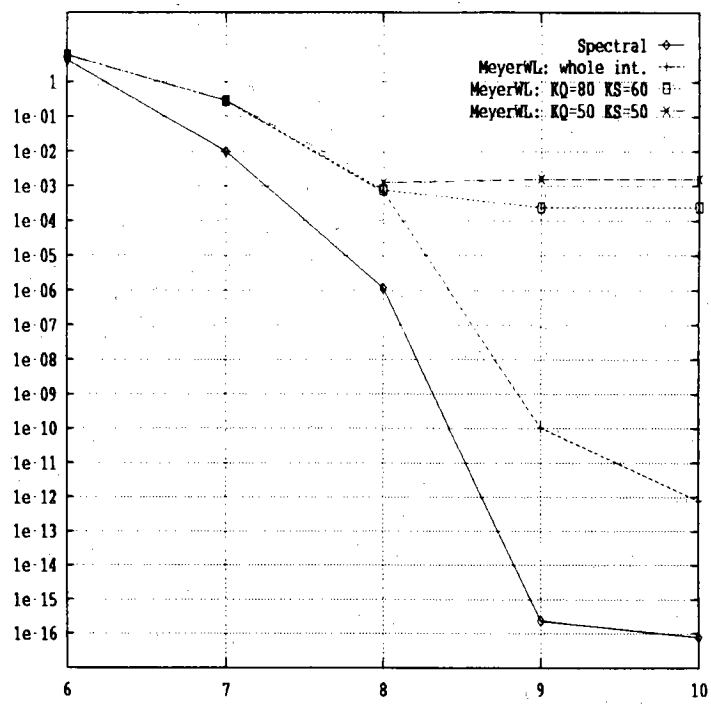

Figure 7: $\|u - u_{ex}\|_2$ in logarithmic scale for the Fourier method, the Meyer wavelet with integration, subtraction on different support (K_Q, K_S).

and f determined such that u_{ex} solves (65). Fixing $\gamma^2 = 16000$ and $\sigma = 150$ (corresponding to $\Delta t = 1.E-2$ which is used later) the computations have been performed in double precision applying the algorithm from section 5.5 with fixed J_r for the regular part and increasing number of scales J. The error of the approximate solution is measured by $\|u - u_{ex}\|$ in the L^2 norm approximated on a grid 2^{J+2} and ploted in Figure 7. The maximum error behaves in avery similar way.

For comparison the results obtained with a classical Fourier method are given as well. These computations aim to indicate which precision can be achieved at most when applying the $O(N_\epsilon)$ algorithm with N_ϵ being the number of active coefficients.

Figure 7 shows first of all the rapid, spectral convergence of the Fourier method. Second, one observes a similar behaviour for the Meyer wavelets when using the quadrature on the whole support. There is some loss in precision due to the smooth transition of the spectrum to zero at its high end. When only part of the wavelets support is taken into account the achievable precision locks at some value corresponding to the truncation error in space. If such a precision is required, however, the present algorithm can furnish the result with less unknowns. An indication on this fact is supplied in Table 2: After having determined all amplitudes d_{ji} and the achieved L^2 precision (Figure 7) we canceled all amplitudes

	$J=8$		$J=9$		$J=10$	
	N_ϵ	$\|u_\epsilon - u_{ex}\|_2$	N_ϵ	$\|u_\epsilon - u_{ex}\|_2$	N_ϵ	$\|u_\epsilon - u_{ex}\|_2$
Fourier	256	1.16 E-06	512	2.33 E-16	1024	7.63 E-17
Meyer $(2^{j+1}, 2^{j+1})$	42	2.03 E-03	356	3.79 E-10	504	7.81 E-13
Meyer (80,60)	42	2.06 E-03	56	5.66 E-04	56	5.65 E-04
Meyer (50,50)	38	3.17 E-03	36	3.87 E-03	36	3.86 E-03

Table 2: Reduction of degrees of freedom and achieved precision for the model problem (65).

$|d_{ji}| < \epsilon = \|u - u_{ex}\|_2$ for each particular case and thus retain a smaller number of them, called N_ϵ, which make up the new solution u_ϵ.
This only results in a degradation of $O(\epsilon)$. Table 2 reports the number of degrees of freedom retained and the corresponding L^2 precision (no manipulation in Fourier space).
We did not consider spline wavelets as they already failed in 5.4 for high precision requirements.

5.7 Discussion

There are two types of numerical errors in the algorithm discussed. One is due to adaption, i.e. due to neglecting coefficients of small absolute value. This is a sort of truncation error. The second one arises from numerical errors in the computation of the coefficients retained. It is the latter one that we were mainly concerned with in this section.
Due to the normalization of the tests in sections 5.2 to 5.5, these results show the relative error in the computation of the wavelet amplitudes d_{ji} of the solution. When aiming to minimize the (absolute) L^2 or Sobolev error of the whole solution one can permit larger relative error if $|d_{ji}|$ is small. This would be possible e.g. for some fine scale amplitudes. The major goal of the described approach was to obtain a satisfactory order of operation counts. To this aim we tried to reduce the numerical location in space and frequency at best. Optimality, of course, cannot be reached due to the Heisenberg principle. The price for the linear operation count of the quadrature is a slight decrease in precision since errors can propagate through the recursion on scales. Since the computation is done from fine to coarse scales which often is related to small to large magnitude of coefficients, i.e. of absolute error, the effect of error propagation through scales seems to be of minor importance in practical computations (with Meyer wavelets).
Finally, it is apparent that the constant in front of the linear order term of the operation count is fairly large. This is due to the large support of the employed wavelets in space. The Daubechies functions having relatively small and compact support do not exhibit a clear separation in frequency space as required here.
The approach adopted here is to start with Meyer wavelets. First of all their localisation is not as bad as believed. Second, they have compact support in frequency space. When subsequently truncating these functions by a cut off in space this compact support is lost, of course. It is however easier to have only one parameter for the required precision namely

	Numerical parameters	results
Spectral	$NX = 256$ points	$v_f(t = 100) = 0.9176$
Meyer Wavelet	$J = 8$ $\epsilon = 10^{-5}$	$v_f(t = 100) = 0.9191$ 122 elements in $A(t = 100)$ 59 elements $> \epsilon$
Meyer Wavelet	$J = 10$ $\epsilon = 10^{-5}$	$v_f(t = 100) = 0.9173$ 128 elements in $A(t = 100)$ 62 elements $> \epsilon$
asymptotic value		$v_f^\infty = 0.908$

Table 3: Comparison of flame velocity and required discretization in one dimension.

the size of the support than additional complications from also truncating in Fourier space first.

6 One dimensional flame computations

6.1 Numerical precision

To start with, the one dimensional problem is solved with the adaptive algorithm for $\alpha = 0.8$, $\beta = 10$, $Le = 1$ with $L_x = 30$, $J_r = 5$ and $\Delta t = 0.01$. The computed flame velocity can then serve as an indicator for the achieved numerical precision. It can be compared to an asymptotic value of [P82] and to the numerical results assembled therein. For comparision we also implemented the non-adaptive spectral Fourier method from [DH90]. The results are assembled in Table 3 (It should be recalled that all computations have been done in single precision.) The result of the spectral method can be considered as being close to optimal. We observe that with the wavelet algorithms the same precision is achieved. Note that the domain, i.e. L_x, is fairly small so that adaptivity does not lead to reducing by more than a half the number of degrees of freedom.
Figure 8 shows cuts in x-direction for T and ω corresponding to the third run in Table 3. They show that the solution is well approximated. Furthermore, it is apparent that the strong nonlinearity of the reaction term leads to very steep behaviour of ω even if T is relatively smooth.

6.2 Higher precision for the species concentration

The criterion choosen in section 4.3 for the choice of the required basis functions is based on a simple thresholding for the magnitude of the wavelet coefficients of the solution. For highly nonlinear problems, however, the precision of the solution can depend in a different way on one or the other unknown, here the temperature and concentration. This is indeed

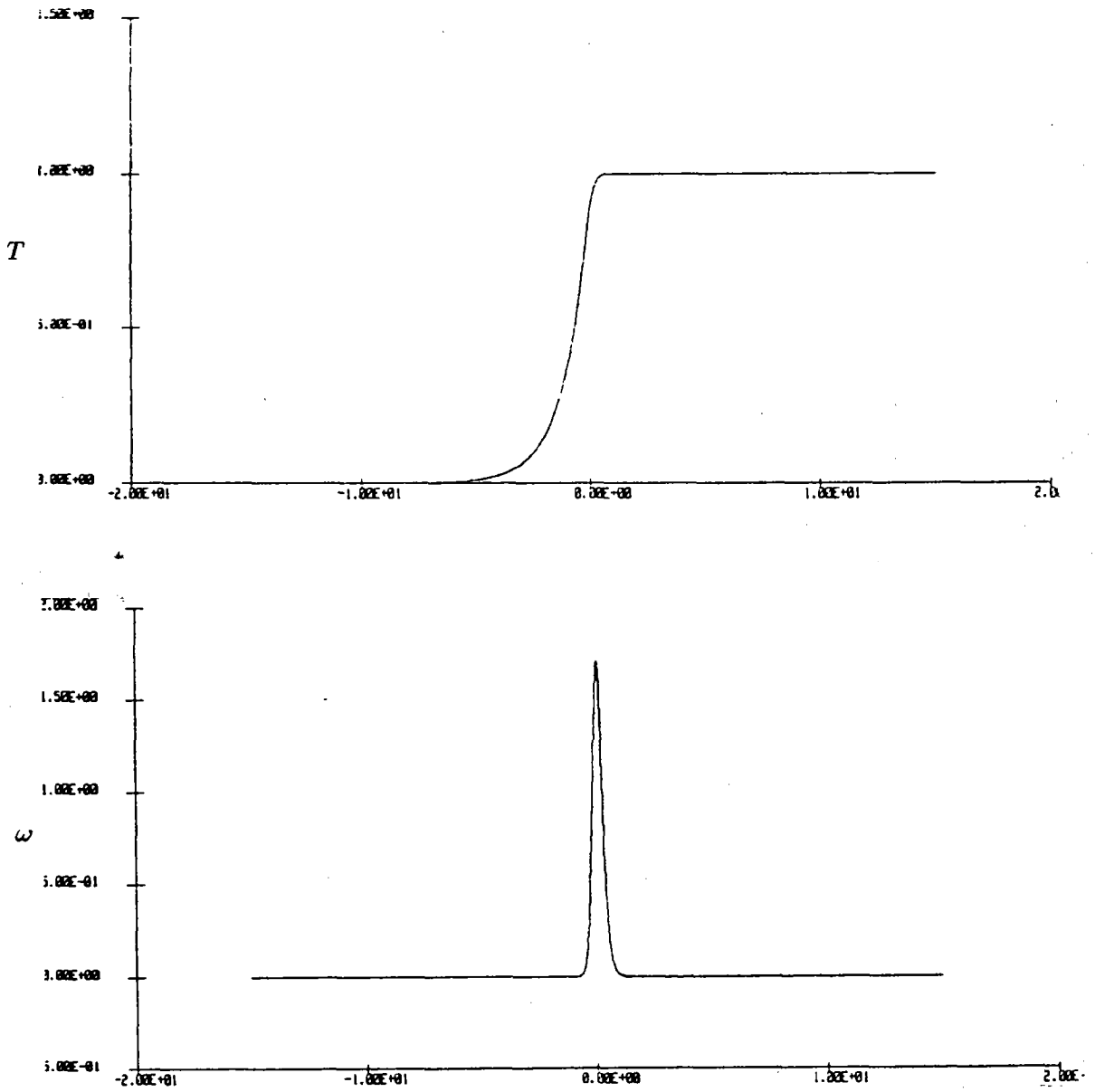

Figure 8: Profiles of T and ω at $t = 100$ for $Le = 1$, $L_x = 30$ with $J_r = 5$, $J = 10$ and $\Delta t = 0.01$.

experienced in the present case: The reaction rate ω in (1) is the product of two factors one of which is linear in Y the other being of exponential type in T. Due to the strong decay of the exponential, oszillations in temperature do not result in oscillations of ω. The linear factor, however, conserves oscillations in this quantity which are the amplified by the factor $\frac{\beta^2}{2Le}$ when the exponential term is O(1). Hence, it is useful to require the concentration to be more precise in order to avoid oscillations in ω which can deteriorate the result. This is done by different thresholds ϵ_T and $\epsilon_Y \leq \epsilon_T$. Moreover, we choose here a spatially varying precision following

$$\epsilon_Y = \epsilon_T - \delta_\epsilon(1 - Y) \tag{67}$$

The result of a sample calculation with $\delta_\epsilon = 0.99\epsilon_T$ is depicted in Figure 9.

6.3 An asside on the periodization technique

In the first half of this section we make some remarks on the choice of the function $S(x)$. Obviously, apart from the requirements indicated in section 2, it has to exhibit some minimal smoothness in order to be well represented on each instantaneous grid. It has furthermore to live on scales more or less related to the regular part of the wavelet bases when the bases is adaptively refined. Imagine as an extremal case $S(x) = T(x,t)$ for some t in a one dimensional calculation. This would lead to vanishing amplitudes for the perturbation $\tilde{T}$ on all scales. For physical reasons the solution could change to some $T(x,t+\Delta t) \neq T(x,t)$, thus $\tilde{T} \neq 0$ in the next time step requiring now large- and fine-scale amplitudes for its representation. Their appearance, however, is no longer related to some notion of neighbouring in coefficient space. Hence, with the present extrapolation technique for the selection of the indices of the active basis functions these cannot be found. Roughly speaking, $S(x)$ should live on lower scales than the unknowns to which the discretization is adapted to. This safely avoids interferrence of $S(x)$ with the adaption process. A consequence is that even in the one dimensional case it is not reasonable trying to optimize $S(x)$ by some choice of parameter with the aim of minimizing the number of degrees of freedom.

Another point can be made on the coordinate transform introduced in section 2 to fix the flame near constant values of x. This is done at the price of additional convective terms that require the use of supplementary test functions θ' which increases the computational cost by doubling the number of scalar products to be calculated and possibly reduces the numerical precision. Let us therefore make some propositions on how to avoid this transform in the present problem while still using periodic functions. We furnish two alternative procedures to periodize (1)-(3).

procedure 1
Solve (6) with $v_f = 0$ for $t = 0$ to $t = t_1 = n_1\Delta t$. Determine the distance

$$L_f = \int_0^{t_1} v_f \, dt \approx \sum_{n=0}^{n_1} v_f^n \Delta t \tag{68}$$

propagated in (here negative) x-direction. Then proceed in the following steps:

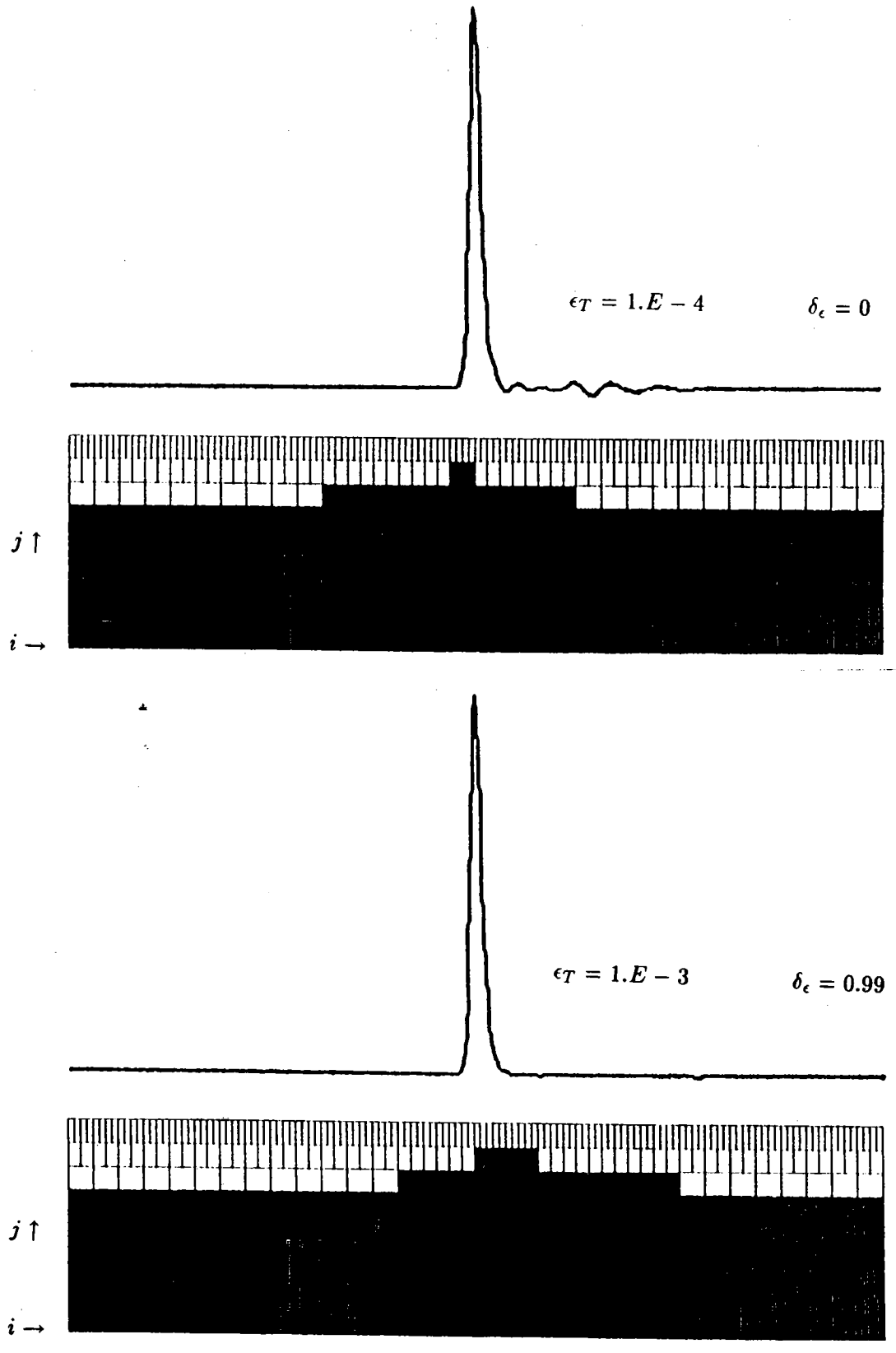

Figure 9: Reaction rate ω where the requirement (67) is met for T or Y with a) $\epsilon_T = 1.E-4$ and $\delta_\epsilon = 0$, b) $\epsilon_T = 1.E-3$ and $\delta_\epsilon = 0.99$.

$$T(x,t_1) = \tilde{T}(x,t_1) + S(x) \tag{69}$$

$$\tilde{T}^*(x) = T(x,t_1) - S(x + r\Delta x) \tag{70}$$

$$L_f^{**} = L_f - r\Delta x \tag{71}$$

$$\tilde{T}^{**}(x) = \begin{cases} \tilde{T}^*(0) & ;x \in [0\,,\, r\Delta x] \\ \tilde{T}^*(x + r\Delta x) & ;x \in [r\Delta x\,,\, 1] \end{cases} \tag{72}$$

$$T^{**}(x,t_1) = \tilde{T}^{**}(x) + S(x) \tag{73}$$

with $r \in I\!N$, and Δx being a unit discussed in a moment. After adding the corresponding steps for Y this solution is then used as a starting point to continue the time integration. For a two step scheme both levels n and $n-1$ are concerned.
Apart from addition and substraction of $S(x)$ everything amounts to shifts. Step (73) uses vanishing derivatives of the unknowns near the boundaries as being done in section 2 before. Observe the invariance of any function in V_j and $W_{j+k}, k > 0$, with respect to shifts of $r/2^{j_1}, r \in Z\!\!Z$, as long as $j_1 \leq j$. Using the basis (56) alows one to benefit from this property reducing (72) to just an index shift by the choice $\Delta x = 1/2^{J_r}$. This is one of the advantages of (56).

procedure 2
This method is similar to the former, but now the flame propagates freely and is periodized with a moving periodic "step function". Define $\tilde{S}(x) = S(x \bmod 1), x \in I\!R$, having a discontinuity at $x = n \in Z\!\!Z$. With t_1, L_f^*, r, and $T(x,t_1)$ as before

$$\tilde{T}^*(x) = \begin{cases} T(x,t_1) - \tilde{S}(x + r\Delta x) & ;x \in [0\,,\, 1 - r\Delta x] \\ \tilde{T}(r\Delta x, t_1) & ;x \in [1 - r\Delta x\,,\, 1] \end{cases} \tag{74}$$

$$\tilde{S}^*(x) = \tilde{S}(x + r\Delta x) \tag{75}$$

$$T^*(x) = \tilde{T}^*(x) + \tilde{S}^*(x) \tag{76}$$

The discontinuity in T and Y now moves through the domain which might be felt as inconvenient. It however avoids index shifts and alows the use of any of the bases (55) or (56).

7 The two dimensional method

7.1 Discretization

Using the time scheme as before we now extend the spatial discretization for solving the entire problem as defined in section 2. This is being done by a tensorproduct

$$\begin{aligned} X_{N,M}^{(x,y)} &= X_N^{(x)} \times X_M^{(y)} \\ Y_{N,M}^{(x,y)} &= Y_N^{(x)} \times Y_M^{(y)} \end{aligned} \tag{77}$$

for the trial and the test space in the method of weighted residuals. These are NM-dimensional subspaces of $L^2(\mathbb{T} \times \mathbb{T})$, here. For $X_N^{(x)}$ and $Y_N^{(x)}$ we take the adaptive discretization developed in section 5. Second,

$$X_M^{(y)} = Y_M^{(y)} = span\{\exp(2\pi iny)\}_{-\frac{M}{2}+1,\ldots,\frac{M}{2}} \tag{78}$$

which amouts to a classical Fourier method in this direction.
The unknowns here are the Fourier coefficients with respect to y of the wavelet series with respect to x. For these, one has to solve a set of one dimensional problems depending on the wavenumber n. The nonlinear right hand side is evaluated in physical space so that the method is a pseudo-spectral one in y-direction. The necessity of executing FFTs in y-direction requires the use of the same discretization in x for all y. This drawback is only felt, however, if the ondulations of the flame are large.

Finally, note that boundary conditions in y can be encorporated e.g. by replacing the Fourier expansion with a Chebyshev sum leading together with the tau-method [GO77] to a quasi-tridiagonal system in coefficient space. It would also be very interesting to employ an adaptive periodic wavelet discretization as in the x-direction to obtain complete adaptivity.

7.2 Computational results for the two dimensional flame front

The results in this section concern the two dimensional thermodiffusive instability. It is the instability of a plane flame front due to different diffusive transport of heat and species the ratio of both being measured by the Lewis number. Starting from a plane flame with a slight pertubation the instability leads to a wrinkled flame as to be seen on the figures below. As an example we choose $L_x = L_y = 35.91$ and $Le = 0.65$. Figure 10 shows Temperature and reaction rate for the transient solution at $t = 50$. The cuts (Figure 11) in the reaction rate demonstrate the strong requirement of local resolution enhancement.

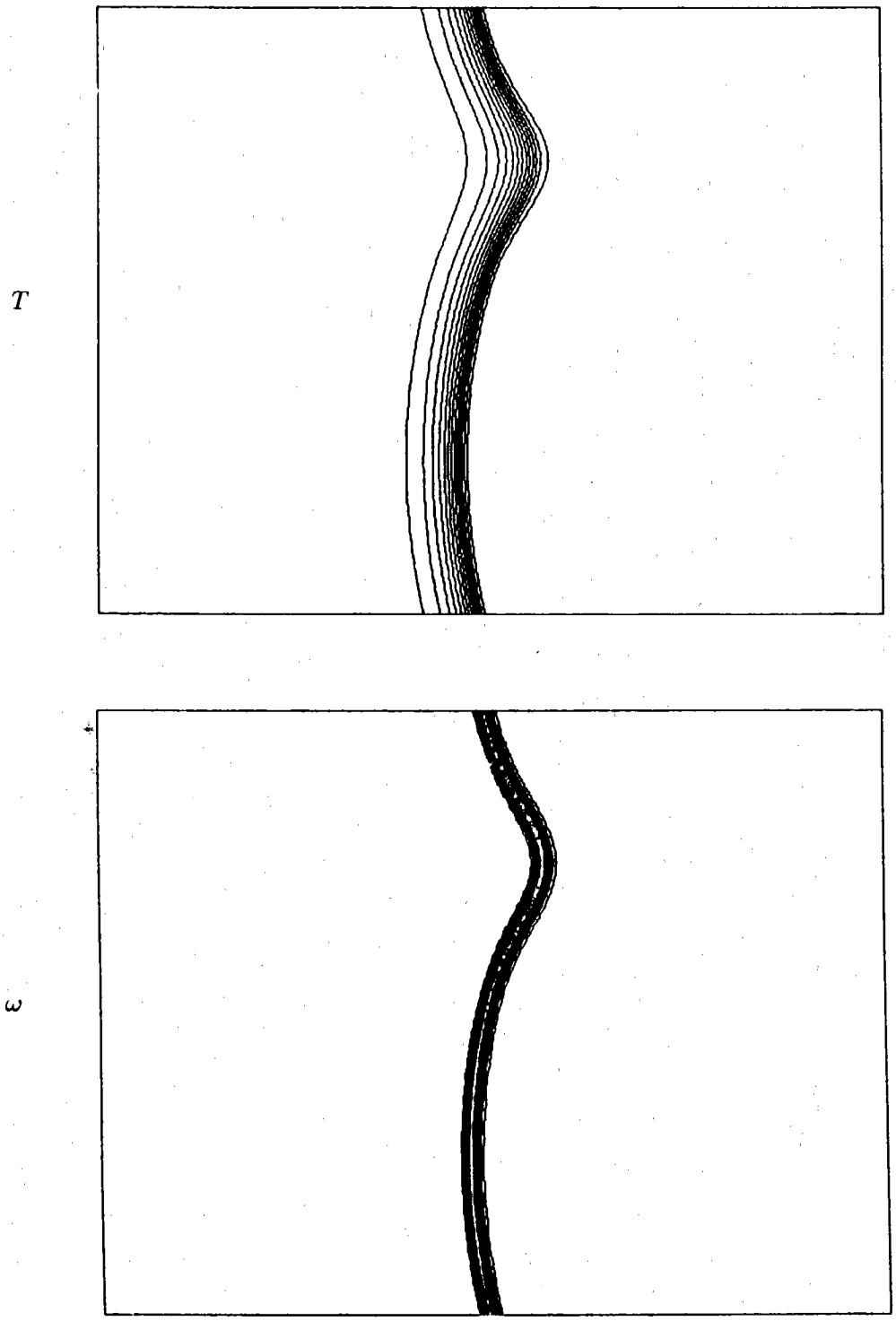

Figure 10: Isolines of T and ω at $t = 50$ for $Le = 0.65$, $L_x = 35.91$, $L_y = 35.91$ with $J_r = 5$, $J = 9$, $M = 48$, $\epsilon_Y = \epsilon_T = 1.E-5$ and $\Delta t = 0.01$.

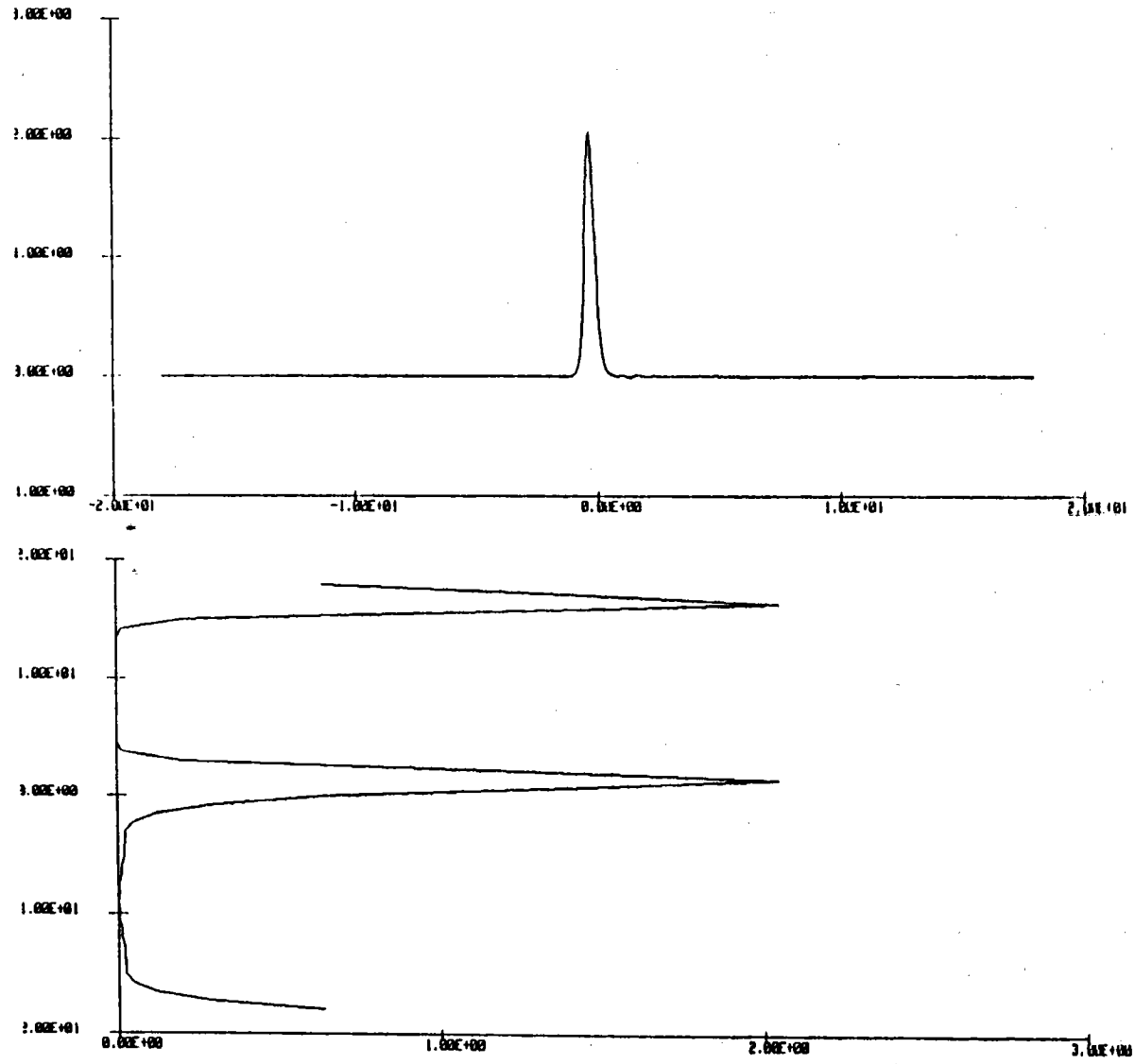

Figure 11: Cuts of ω at $x = 0$ and $y = 0$ corresponding to Figure 10.

Appendix A Spline wavelets

The nonperiodic spline multiresolution of $L^2(\mathbb{R})$ is defined by the following formulas from [PB89]

$$\hat{S}(\xi) = \frac{\sin^m(\pi\xi)}{(\pi\xi)^m\, P_{\frac{m}{2}-1}(\sin^2(\pi\xi))} \tag{79}$$

$$\hat{\phi}(\xi) = \frac{\sin^m(\pi\xi)}{(\pi\xi)^m \sqrt{P_{m-1}(\sin^2(\pi\xi))}} \tag{80}$$

$$\hat{\psi}(\xi) = \frac{\sin^{2m}(\pi\xi/2)}{(\pi\xi/2)^m} \sqrt{\frac{P_{m-1}(\cos^2(\pi\xi/2))}{P_{m-1}(\sin^2(\pi\xi/2))\; P_{m-1}(\sin^2(\pi\xi))}}\; e^{-i\xi\pi} \tag{81}$$

for the cardinal Lagrange spline, the scaling function, and the mother-wavelet, respectively. The m-th order polynomial P_m

$$P_m(x) = \sum_{i=0}^{m} a_i^m\, x^i \tag{82}$$

is determined by

$$\frac{P_{m-1}(\sin^2 z)}{\sin^{2m} z} = \sum_{n\in\mathbb{Z}} \frac{1}{(z+n\pi)^{2m}} \tag{83}$$

and can be calculated via

$$a_0^r = 1 \qquad\qquad r = 0,\ldots,m \tag{84}$$

$$a_i^r = \frac{1}{r(2r+1)} \left((r-i)(2r-2i+1)\, a_i^{r-1} - 2(r-i+1)^2\, a_{i-1}^{r-1} \right) \qquad i = 1,\ldots,r \tag{85}$$

The quadrature mirror filters g, h and the interpolation filter L are obtained from the 2π-periodic functions

$$L(\omega) = \frac{\hat{S}(\omega)}{\hat{\phi}(\omega)} \qquad G(\omega) = \frac{\hat{\psi}(2\omega)}{\hat{\phi}(\omega)} \qquad H(\omega) = \frac{\hat{\phi}(2\omega)}{\hat{\phi}(\omega)} \tag{86}$$

that read for the above expressions

$$L(\omega) = \frac{\sqrt{P_{m-1}(\sin^2 \pi\omega)}}{P_{\frac{m}{2}-1}(\sin^2 \pi\omega)} \tag{87}$$

$$H(\omega) = \sqrt{2}\, \cos^m(\pi\omega) \sqrt{\frac{P_{m-1}(\sin^2 \pi\omega)}{P_{m-1}(\sin^2(2\pi\omega))}} \tag{88}$$

$$G(\omega) = \sqrt{2}\, \sin^m(\pi\omega) \sqrt{\frac{P_{m-1}(\cos^2 \pi\omega)}{P_{m-1}(\sin^2(2\pi\omega))}}\; e^{-2i\pi\omega} \tag{89}$$

Sampling in frequency space as described in section 2 and additional scaling for L leads to the periodic filters in Fourier space

$$(\widehat{L_J})_k = \frac{1}{2^{3J/2}} L(\frac{k}{2^J}) \qquad (\widehat{h_j})_k = \frac{1}{2^j} H(\frac{k}{2^j}) \qquad (\widehat{g_j})_k = \frac{1}{2^j} G(\frac{k}{2^j}) \tag{90}$$

required for the wavelet transform in $L^2(\mathbb{T})$.

Appendix B Meyer wavelets

The Meyer wavelets used in the present calculations are defined by the following formula that are taken from [P91],

$$\hat{\phi}(\xi) = \begin{cases} 1 & ;|\xi| \leq \frac{1}{3} \\ \cos(\frac{\pi}{2}\nu(3|\xi|-1)) & ;\frac{1}{3} \leq |\xi| \leq \frac{2}{3} \\ 0 & ;\text{elsewhere} \end{cases} \tag{91}$$

$$\hat{\psi}(\xi) = \begin{cases} \exp(-i\pi\xi)\cos(\frac{\pi}{2}\nu(-3|\xi|+2)) & ;\frac{1}{3} \leq |\xi| \leq \frac{2}{3} \\ \exp(-i\pi\xi)\cos(\frac{\pi}{2}\nu(\frac{3}{2}|\xi|-1)) & ;\frac{2}{3} \leq |\xi| \leq \frac{4}{3} \\ 0 & ;\text{elsewhere} \end{cases} \tag{92}$$

The cardinal Lagrange function can be obtained from $\hat{\phi}$ by

$$\hat{S}(\xi) = \frac{\hat{\phi}(\xi)}{\hat{\phi}^*(\xi)} \tag{93}$$

[Wa92], where $\hat{\phi}^*(\xi)$ denotes the sampled scaling function

$$\hat{\phi}^*(\xi) = \sum_{n \in \mathbb{Z}} \phi(n) \exp(-2\pi i \xi n) \tag{94}$$

For the smooth "step function" ν we have choosen the one which according to [D92] gives best localisation in physical domain.

$$\nu(x) = x^4(35 - 84x + 70x^2 - 20x^3) \tag{95}$$

The quadrature mirror filters $\hat{g}$, $\hat{h}$ and the interpolation filter for the periodic and nonperiodic case are determined as in Appendix A.

References

[ABMD92] M. Antonini, M. Barlaud, P. Mattieu, I. Daubechies, *Image coding using wavelet transform*, IEEE Trans. Image Proc., vol. 1, 205-220, 1992.

[BMP91] E. Bacry, S. Mallat, G. Papanicolaou, *A wavelet based space-time adaptive numerical method for partial differential equations*, Technical report No 591, New York University, 1991.

[BHP90] C. Basdevant, M. Holschneider, V. Perrier, *Méthode des ondelettes mobiles*, C.R.Acad.Sci. Paris, t.310, 647-652, 1990.

[BL88] F. Benkaldoun, B. Larrouturou, *Numerical Analysis of the two-dimensional thermodiffusive model for flame propagation*, RAIRO, Modelisation Math. Anal. Numer., vol. 22, 535-560, 1988.

[BF70] W.B. Bush, F.E. Fendel, *Asymptotic analysis of laminar flame propagation for general Lewis number*, Combust. Sci. Tech., vol. 1, 421-428, 1970.

[BCR91] G. Beylkin, R. Coifman, V. Rokhlin, *Fast wavelet transforms and numerical algorithms I*, Comm. Pure Appl. Math., vol. 44, 141-183, 1991.

[Ch93] E. Charton, *Algorithme BCR pour EDP*, lecture at the Workshop *Ondelettes et EDP, aspets adaptatifs*, Marseille, 1993.

[C92] C.K. Chui, *An introduction to wavelets*, Academic Press, New York, 1992.

[CHQZ88] C. Canuto, M.Y. Hussaini, A. Quarteroni, T.A. Zang, *Spectral methods in fluid dynamics*, Springer-Verlag, 1988.

[DK92] W. Dahmen, A. Kunoth, *Multilevel preconditioning*, Numer. Math., 63, 315-344, 1992.

[D90] I. Daubechies, *The wavelet transform, time frequency localization and signal analysis*, IEEE Trans. Inform. Theory, vol. 36, 961-1005, 1990.

[D92] I. Daubechies, *Ten lectures on wavelets*, SIAM, Philadelphia, 1992.

[DH90] B. Denet, P. Haldenwang : *A local extinction of the thermo-diffusive premixed flame at low Lewis number*, in A. Dervieux, B. Larrouturou (Eds.), *Numerical combustion*, Lecture Notes in Physics, vol. 351, Springer-Verlag, 1990.

[DJL] R. DeVore, B. Jawerth, B. Lucier, *Image compression through wavelet transform coding*, preprint, University of South Carolina.

[EGP89] U. Ehrenstein, H. Guillard, R. Peyret, *Flame computations by the Chebyshev multi domain method*, Int. J. Numer. Methods Fluids, vol. 9, 499-515, 1989.

[F72] B.A. Finlayson *The method of Weighted Residuals and Variational Principles*, Academic Press, 1972.

[GLRT90] R. Glowinski, R.W. Lawton, M. Ravachol, E. Tennenbaum, *Wavelet solution of linear and nonlinear elliptic, parabolic, and hyperbolic problems in one space dimension*, in Proc. Ninth Int. Conf. on Comp. Meth. in Appl. Sci. and Eng., R. Glowinski, A. Lichnewsky (eds.), SIAM Publ., Philadelphia, PA, 1990.

[GO77] , D. Gottlieb, S.A. Orszag, *Numerical analysis of spectral methods*, SIAM, Philadelphia, 1970.

[GM84] A. Grossmann, J. Morlet, *Decomposition of Hardy functions into square integrable wavelets of constant shape* , SIAM J. Math. Anal., vol. 15, 723-736, 1984.

[HT89] M. Holschneider, Ph. Tchamitchian, *Regularité locale de la fonction non-differentiable de Riemann*, in *Les ondelettes en 1989*, Lecture Notes in Mathematics, P.G. Lemarié (ed.), Springer, 1989.

[JL92] S. Jaffard, Ph. Lorençot, *Orthonormal Wavelets, Analysis of Operators, and Applications to Numerical Analysis*, in C.K. Chui (ed.), *Wavelets: A Tutorial in Theory and applications*, Acad. Press, 1992.

[LL93] S. Lazaar, J. Liandrat, *Inversion des opérateurs elliptiques dans des bases d'ondelettes*, lecture at the Workshop *Ondelettes et EDP, aspets adaptifs*, Marseille, 1993.

[LT90] J. Liandrat, Ph. Tchamitchian, *Resolution of the 1D regularized Burgers equation using a spatial wavelet approximation algorithm and numerical results*, ICASE report, 1990.

[LPT91] J. Liandrat, V. Perrier, Ph. Tchamitchian, *Numerical resolution of non linear partial differential equations using the wavelet approach*, in *Wavelets and their applications*, B. Rushkai (Ed.), Publ. Jones and Barlett, 1991.

[MPR91] Y. Maday, V. Perrier, J.Ch. Ravel, *Adaptivité dynamique sur bases d'ondelettes pour l'approximation d'équations aux derivées partielles*, C.R.Acad.Sci. Paris, t.312, I, pp. 405-410, 1991.

[MPR92] Y. Maday, V. Perrier, J.Ch. Ravel, *Adaptivité par ondelettes: conditions aux limites et dimensions suppérieures*, C.R.Acad.Sci. Paris, t.315, I, pp. 85-90, 1992.

[Ma89] S. Mallat, *Multiresolution approximation and wavelets*, Trans. Am. Math. Soc., vol. 315, 69-88, 1989.

[MaHw92] S. Mallat, W.L. Hwang, *Singularity detection and processing with wavelets*, IEEE Trans. Inform. Theory, vol. 38, 617-643, 1992.

[Me89] Y. Meyer, *Orthonormal wavelets*, in J.M. Combes, A. Grossmann, Ph. Tchamitchian (eds.), *Wavelets, time-frequency methods and phase space*, Springer, 21-37, 1989.

[Me90a] Y. Meyer, *Ondelettes et applications*, Journée annuelle de la Societé Mathématique de France, 1990.

[Me90] Y. Meyer, *Ondelettes et operateurs I*, Herman, Paris, 1990.

[P91] V. Perrier, *Ondelettes et simulation numerique*, thesis, University Paris IV, 1991.

[PB89] V. Perrier, C. Basdevant, *La décomposition en ondelettes périodiques, un outil pour l'analyse de champs inhomogènes. Théorie et algorithmes* , Rech. Aérosp., 53-67, 1989-3.

[P82] N. Peters, *Discussion of test problem A*, in N. Peters, J. Warnatz, (eds.), *Numerical methods in laminar flame propagation*, Notes on numerical fluid mechanics, Vol.6, Vieweg, 1982.

[RV91] O. Rioul, M. Vetterli, *Wavelets and signal processing*, IEEE SP Magazine, 14-38, Oct. 1991.

[T89] Ph. Tchamitchian, *Bases d'ondelettes et integrales singulières: Analyse des fonctions et calcul sur les opérateurs*, Habilitation, Marseille, 1989.

[Wa92] G. Walter, *A sampling theorem for wavelet subspaces*, IEEE Trans. Inform. Theory, vol. 38, 881-884, 1992.

[Wi85] F.A. Williams, *Combustion theory*, Benjamin/Cummings, Menlo Park, California, 1985.

J. Fröhlich, K. Schneider
Fachbereich Mathematik
University of Kaiserslautern
Erwin-Schrödinger-Straße
67663 Kaiserslautern
Germany